Hyperfine-induced frequency shifts for the candidate clock transitions in the $^{61}Ni^{12+}$ ion

Ting-xian Zhang,[1,*] Cheng-bin Li,[2,†] and Ting-yun Shi[2,‡]

[1]*School of Science, Lanzhou University of Technology, Lanzhou 730050, People's Republic of China*

[2]*State Key Laboratory of Magnetic Resonance and Atomic and Molecular Physics, Innovation Academy for Precision Measurement Science and Technology, Chinese Academy of Sciences, Wuhan 430071, People's Republic of China*

(Received 25 June 2024; accepted 13 August 2024; published 3 September 2024)

The $^{61}Ni^{12+}$ ion is a promising candidate for a novel ultraprecise optical clock, owing to its two clock transitions with narrow natural linewidth between levels with low degeneracy. Using the multiconfiguration Dirac-Hartree-Fock (MCDHF) method, we calculated the hyperfine-induced Landé g factors for the $^3P_0$ $F = 3/2$ and $^3P_{1,2}$ $F = 1/2$ states, as well as the hyperfine-induced electronic quadrupole moment of the $^3P_0$ $F = 3/2$ state in the $^{61}Ni^{12+}$ ion. The effects of the electron correlations and relativistic effects on the concerned atomic parameters were evaluated in detail based on the active space approach. It is found that the valence-valence and core-valence electron correlations have the dominant influence on the atomic parameters concerned, while the core-core and the higher-order correlations are non-negligible for evaluating the uncertainties. Additionally, the relative quadratic Zeeman shifts, the relative electric quadrupole shift, and the corrections arising from the hyperfine-induced effect were evaluated. It is demonstrated that the hyperfine interaction strictly eliminates the electric quadrupole shift of the M1 transition $3s^23p^4\ {}^3P_1 - {}^3P_2$, and significantly reduces the electric quadrupole frequency shift for the E2 transition $3s^23p^4\ {}^3P_0 - {}^3P_2$ by a factor of 4×10^{-6}. The hyperfine-induced corrections to the relative quadratic Zeeman shifts are factors of 2×10^{-4} and 6×10^{-7} for the M1 and E2 transition, respectively. It means that the hyperfine-induced effects need to be identified precisely for an ultraprecise $^{61}Ni^{12+}$ optical clock aiming for a precision better than 10^{-19} when the magnetic field exceeds 1 μT or the gradient of the environmental electric field exceeds 10^8 V/m^2.

DOI: 10.1103/PhysRevA.110.032801

I. INTRODUCTION

The extraordinary precision afforded by optical clocks not only facilitates the improvement of time standards, but also enables the testing of fundamental physics, such as looking for changes in fundamental constants over time, measuring gravity redshift, and probing the existence of forces beyond the Standard Model [1–4]. Up to now, the fractional uncertainties of ^{171}Yb, $^{171}Yb^+$, ^{87}Sr, and $^{40}Ca^+$ clocks have been achieved at a level of 10^{-18} [5–8], and at 10^{-19} for the $^{27}Al^+$ clock [9]. Compared to the neutral atoms and singly charged ions, highly charged ions (HCIs) possess extremely narrow optical transitions that are insensitive to the external perturbations and more sensitive to the variation of the fine structure constant α, due to the shrunk electronic cloud and enhanced relativity effect with the increasing of the ion charge. In recent years, nearly 70 HCIs have been suggested as candidates for ultraprecise optical clocks and exploring new physics beyond the Standard Model [10–21]. Meanwhile, the HCI optical clock experiments have made substantial progress [22–24]. For instance, the sympathetic cooling and quantum logic spectroscopy of HCIs have been applied for the Ar^{13+} ion [22,23]. The Ar^{13+} clock with an uncertainty of 2.2×10^{-17} has been achieved, while the associated instability of $2.6 \times 10^{-14}/\sqrt{\tau}$ is limited mainly by the natural linewidth (∼16 Hz) of the clock transition [24]. Additionally, optical clocks based on the HCI with narrow clock transition, such as Ni^{12+}, Pd^{12+}, Pr^{9+}, Nd^{9+}, and Pb^{41+}, are also being developed [25–30].

The Ni^{12+} ion is one of the most promising candidates for a novel ultraprecise optical clock, since it provides two optical clock transitions with narrow natural linewidths within its simple energy level structures, the electric quadrupole (E2) transition at 498 nm $3s^23p^4\ {}^3P_0 - {}^3P_2$ and the magnetic dipole (M1) transition at 512 nm $3s^23p^4\ {}^3P_1 - {}^3P_2$ [26]. In particular, the high-quality factor of the E2 transition at 7.5×10^{16} is beneficial to provide high stability for the optical clock, which is advantageous for its precision and accuracy in timekeeping. Furthermore, the M1 transition serves not only as a candidate optical clock transition to demonstrate the HCI clock but also as a logic transition for detecting the E2 clock transition [29]. The electric quadrupole shift, caused by the interaction between the electric quadrupole moments of the clock states and the gradient of the electric field, is one of the main systematic shifts in the atomic clock. Compared with bosonic Ni isotopes, the fermionic ^{61}Ni ($I = 3/2$) isotope can substantially suppress the electric quadrupole frequency shift of the clock transitions by selecting clock transitions between the particular hyperfine levels [27,31]. As shown in

*Contact author: tingxianzhang@lut.edu.cn
†Contact author: cbli@wipm.ac.cn
‡Contact author: tyshi@wipm.ac.cn

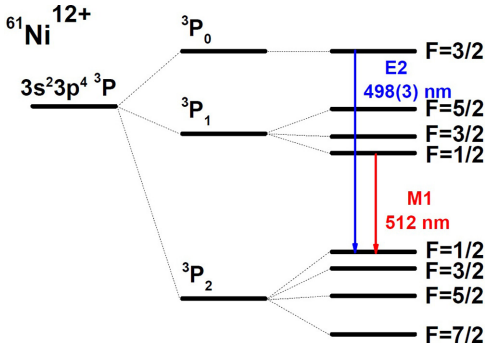

FIG. 1. Clock transitions in the $^{61}Ni^{12+}$ ion.

Fig. 1, the clock transitions corresponding to the $^{61}Ni^{12+}$ ion are $3s^23p^4\ {}^3P_0\ F = 3/2 - {}^3P_2\ F = 1/2$ and $3s^23p^4\ {}^3P_1\ F = 1/2 - {}^3P_2\ F = 1/2$. In this way, the electric quadrupole frequency shift of the M1 transition will be strictly removed, and the electric quadrupole frequency shift of E2 transition will be reduced significantly. However, the hyperfine interaction caused by the coupling of the spin of the ^{61}Ni nucleus to electrons breaks the spatial symmetry of the electron cloud, and thus leads to a mixing between the states with the same parity but different angular momenta. This introduces a slight sensitivity to the perturbations from electromagnetic field and systematic frequency shifts for an optical clock. For instance, the hyperfine interaction results in nonzero Landé g factors for the $^3P_0$ clock state of the $^{27}Al^+$ and ^{87}Sr clock [32]. In fact, the "hyperfine-induced" effect will influence the frequency shifts of the clock transitions of the $^{61}Ni^{12+}$ ion, but there has been no investigation of it.

In this work, we carried out *ab initio* calculations on the hyperfine-induced Landé g factors of $^3P_0\ F = 3/2$ and $^3P_{1,2}\ F = 1/2$ states, and the electronic quadrupole moment of the $^3P_0\ F = 3/2$ state involved in clock transitions of $^{61}Ni^{12+}$ ion, using the MCDHF method. The electron correlations, not only in the valence shell but also those related to the core, were taken into account systematically based on the active space approach, as high-quality wave functions are required for accurate determination of hyperfine-induced Landé g factors and electronic quadrupole moment. In addition, the relative quadratic Zeeman shifts, the relative electric quadrupole shifts, and the correction due to the hyperfine-induced effect on these shifts were evaluated. This work is expected to support the experimental investigations of the $^{61}Ni^{12+}$ ion optical clock.

II. THEORETICAL METHOD

A. Hyperfine interaction

The hyperfine interaction, denoted as $H_{\rm hfs}$, is the interaction between the electrons and the electromagnetic multipole moments of the nucleus. For an N-electron atom system with the nonzero nuclear spin, its Hamiltonian can be represented as a sum of $H_{\rm hfs}$ and the relativistic Dirac-Coulomb-Breit (DCB) Hamiltonian $H_{\rm DCB}$,

$$H = H_{\rm DCB} + H_{\rm hfs}. \tag{1}$$

The DCB Hamiltonian is given by

$$H_{\rm DCB} = \sum_{i=1}^{N}[c\,\boldsymbol{\alpha}_i\cdot\boldsymbol{p}_i + (\beta_i - 1)c^2 + V_{\rm nuc}(r_i)] + \sum_{i>j}^{N}\left[\frac{1}{r_{ij}} + B_{ij}\right], \tag{2}$$

where c is the speed of light in vacuum, $\boldsymbol{\alpha}_i$ and β_i are the 4×4 Dirac matrices, $V_{\rm nuc}(r_i)$ is the monopole part of the electron-nucleus interaction, $\frac{1}{r_{ij}}$ is the Coulomb interaction, and B_{ij} is the Breit interaction in the frequency-independent limit, given by

$$B_{ij} = -\frac{1}{2r_{ij}}\left[\boldsymbol{\alpha}_i\cdot\boldsymbol{\alpha}_j + \frac{(\boldsymbol{\alpha}_i\cdot\boldsymbol{r}_{ij})(\boldsymbol{\alpha}_j\cdot\boldsymbol{r}_{ij})}{r_{ij}^2}\right]. \tag{3}$$

The hyperfine interaction $H_{\rm hfs}$ is represented as a scalar product of two spherical tensors with the rank of k,

$$H_{\rm hfs} = \sum_{k\geqslant 1}\boldsymbol{T}^{(k)}\cdot\boldsymbol{M}^{(k)}, \tag{4}$$

where $\boldsymbol{T}^{(k)}$ and $\boldsymbol{M}^{(k)}$ act on the electronic and nuclear space, respectively [33]. The $k = 1$ and $k = 2$ terms describe the magnetic dipole and electric quadrupole hyperfine interactions, respectively. The higher-order terms with $k \geqslant 2$ are small and neglected in this work. For an N-electron atom, the electronic tensor operators $\boldsymbol{T}^{(1)}$ and $\boldsymbol{T}^{(2)}$ read

$$\boldsymbol{T^{(1)}} = \sum_{j=1}^{N}\boldsymbol{t}^{(1)}(j) = \sum_{j=1}^{N} -\mathrm{i}\alpha(\boldsymbol{\alpha}_j\cdot\mathbf{l}_j\boldsymbol{C}^{(1)}(j))r_j^{-2} \tag{5}$$

and

$$\boldsymbol{T^{(2)}} = \sum_{j=1}^{N}\boldsymbol{t}^{(2)}(j) = \sum_{j=1}^{N} -\boldsymbol{C}^{(2)}(j)r_j^{-3}, \tag{6}$$

where i is the imaginary unit, α is the fine-structure constant, and $\mathbf{l}_j$ is the orbital angular momentum operator. $\boldsymbol{C}^{(1)}$ and $\boldsymbol{C}^{(2)}$ are spherical tensor operators with the components related to the spherical harmonics as $C_q^{(k)} = \sqrt{\frac{4\pi}{2k+1}}Y_{kq}$. The magnetic dipole moment μ_I and electronic quadrupole moment Q of the nucleus are related to the matrix elements of the nuclear tensor operators $\boldsymbol{M}^{(1)}$ and $\boldsymbol{M}^{(2)}$ through [34]

$$\mu_I = \sqrt{2I+1}\begin{pmatrix} I & 1 & I \\ -I & 0 & I\end{pmatrix}\langle\Upsilon I||\boldsymbol{M}^{(1)}||\Upsilon I\rangle\,, \tag{7}$$

$$Q_I = 2\sqrt{2I+1}\begin{pmatrix} I & 2 & I \\ -I & 0 & I\end{pmatrix}\langle\Upsilon I||\boldsymbol{M}^{(2)}||\Upsilon I\rangle. \tag{8}$$

The values of the magnetic dipole moment and electronic quadrupole moment of ^{61}Ni, $\mu_I = -0.75002\,\mu_N$ and $Q = 0.162$ b, were taken from the table by Stone [35].

The hyperfine interaction causes the electronic angular momentum $\boldsymbol{J}$ to couple with the nuclear spin $\boldsymbol{I}$ and form a total angular momentum $\boldsymbol{F}$, i.e., $\boldsymbol{F} = \boldsymbol{I} + \boldsymbol{J}$. In this case, F and M_F are good quantum numbers, and the wave functions of the atomic system $|FM_F\rangle$ are expressed as

$$|FM_F\rangle = \sum_{\Gamma' J'} d_{\Gamma' J'}|\Upsilon\Gamma' IJ' FM_F\rangle, \tag{9}$$

where

$$|\Upsilon\Gamma IJFM_F\rangle = \sum_{M_I M_J} \langle IJM_I M_J|IJFM_F\rangle |\Upsilon IM_I\rangle |\Gamma JM_J\rangle. \tag{10}$$

Here $\langle IJM_I M_J|IJFM_F\rangle$ is the Clebsch-Gordan coefficient, and $|\Upsilon IM_I\rangle$ and $|\Gamma JM_J\rangle$ are wave functions of the nucleus and the electrons in the atom, respectively, in which Υ and Γ represent the additional quantum numbers for describing nuclear and electronic states uniquely. Comparing with the fine structure split, the hyperfine interaction is so weak that it can be treated as a perturbation. In the first-order perturbation approximation, hyperfine-induced mixing coefficients are

$$d^{(1)}_{\Gamma' J'} = \frac{\langle \Upsilon\Gamma' IJ'FM_F|H_{\rm hfs}|\Upsilon\Gamma IJFM_F\rangle}{E_{\Upsilon\Gamma IJFM_F} - E_{\Upsilon\Gamma' IJ'FM_F}}, \tag{11}$$

where the primes label the perturbing states. The matrix elements for the magnetic dipole and the electric quadrupole hyperfine interaction are

$$\begin{aligned}&\langle \Upsilon\Gamma IJFM_F|\boldsymbol{T}^{(1)}\cdot\boldsymbol{M}^{(1)}|\Upsilon\Gamma' IJ'FM_F\rangle \\ &= (-1)^{I+J+F}\begin{Bmatrix} I & J & F \\ J' & I & 1\end{Bmatrix} \\ &\quad\times\sqrt{2J+1}\sqrt{2I+1}\langle\Gamma J\|\boldsymbol{T}^{(1)}\|\Gamma' J'\rangle\langle\Upsilon I\|\boldsymbol{M}^{(1)}\|\Upsilon I\rangle,\end{aligned} \tag{12}$$

and

$$\begin{aligned}&\langle \Upsilon\Gamma IJFM_F|\boldsymbol{T}^{(2)}\cdot\boldsymbol{M}^{(2)}|\Upsilon\Gamma' IJ'FM_F\rangle \\ &= (-1)^{I+J+F}\begin{Bmatrix} I & J & F \\ J' & I & 2\end{Bmatrix} \\ &\quad\times\sqrt{2J+1}\sqrt{2I+1}\langle\Gamma J\|\boldsymbol{T}^{(2)}\|\Gamma' J'\rangle\langle\Upsilon I\|\boldsymbol{M}^{(2)}\|\Upsilon I\rangle,\end{aligned} \tag{13}$$

respectively.

B. Zeeman effect of hyperfine levels

The interaction between the atom and magnetic field $\boldsymbol{B}$ can be described by the Hamiltonian $H_{\rm m}$ [36,37],

$$H_{\rm m} = -(\boldsymbol{\mu_I} + \boldsymbol{\mu}_e)\cdot\boldsymbol{B}, \tag{14}$$

where $\boldsymbol{\mu_I}$ is the nuclear magnetic moment. The interaction between the nuclear magnetic moment and the magnetic field, $-\boldsymbol{\mu_I}\cdot\boldsymbol{B}$, is related to the nuclear g factor of $g_I = -(m_e/m_p)(\mu_I/I\mu_N)$, where m_e and m_p are the electron and proton masses, respectively. For the ^{61}Ni isotope, $g_I = -2.72\times10^{-4}$. The electronic magnetic moment $\boldsymbol{\mu_e}$ that includes the Schwinger quantum electrodynamic (QED) correction is given by

$$\boldsymbol{\mu_e} = \boldsymbol{N}^{(1)} + \Delta\boldsymbol{N}^{(1)} \tag{15}$$

and

$$\boldsymbol{N}^{(1)} = \sum_{j=1}^{N}\boldsymbol{n}^{(1)}(j) = -\sum_{j=1}^{N}\frac{\sqrt{2}i}{2\alpha}(\boldsymbol{\alpha}_j\cdot\mathbf{l}_j\boldsymbol{C}^{(1)}(j))r_j, \tag{16}$$

$$\Delta\boldsymbol{N}^{(1)} = \sum_{j=1}^{N}\Delta\boldsymbol{n}^{(1)}(j) = \sum_{j=1}^{N}\frac{(g_s-2)}{2}\beta_j\boldsymbol{\Sigma}_j, \tag{17}$$

where $\boldsymbol{\Sigma}_j$ is the relativistic spin matrix, and $g_s = 2.00232$ stands for the g factor of the electron spin corrected by QED effects.

In the weak-magnetic-field approximation, $H_{\rm m} \ll H_{\rm hfs}$, the energy shift of a given hyperfine level $|FM_F\rangle$ can be determined by the perturbation theory,

$$\begin{aligned}\Delta E^{(1)}_{\rm m} &= \frac{1}{2}\langle FM_F|\boldsymbol{N}^{(1)} + \Delta\boldsymbol{N}^{(1)}|FM_F\rangle B \\ &= M_F\frac{F(F+1)+J(J+1)-I(I+1)}{2F(F+1)} \\ &\quad\times\frac{\langle\Gamma J\|\boldsymbol{N}^{(1)}+\Delta\boldsymbol{N}^{(1)}\|\Gamma J\rangle}{\sqrt{J(J+1)}}B \\ &= M_F\frac{F(F+1)+J(J+1)-I(I+1)}{2F(F+1)}g_J\frac{B}{2} \\ &= M_F g_F\frac{B}{2},\end{aligned} \tag{18}$$

where g_J and g_F are Landé g factors for the fine and hyperfine states. Substituting Eq. (9) into the equation above, the g_F can be written as

$$\begin{aligned}g_F &\approx \frac{\langle\Upsilon\Gamma IJFM_F|N^{(1)}_0 + \Delta N^{(1)}_0|\Upsilon\Gamma IJFM_F\rangle}{M_F} \\ &\quad + 2\sum_{\Gamma' J'} d^{(1)}_{\Gamma' J'}\frac{\langle\Upsilon\Gamma IJFM_F|N^{(1)}_0+\Delta N^{(1)}_0|\Upsilon\Gamma' IJ'FM_F\rangle}{M_F} \\ &= g^{(0)}_F + \delta g^{(1)}_{F\,\rm hfs}.\end{aligned} \tag{19}$$

The last term $\delta g^{(1)}_{F\,\rm hfs}$ represents a hyperfine-induced Landé g factor. Only the states belonging to the $3s^2 3p^4$ configuration are treated as perturbing states in practical calculations, neglecting others because of their fractional contribution due to large energy intervals. For instance, the contributions from states above $3s^2 3p^4$ were estimated to be less than 10^{-10} for the $\delta g^{(1)}_{F\,\rm hfs}$ of concerned states in the $^{61}Ni^{12+}$ ion.

Generally, the second-order Zeeman effects also should be considered for evaluating the Zeeman shift of the clock transition frequency. For an atomic state $|FM_F\rangle$, the second-order Zeeman shift is given by

$$\begin{aligned}\Delta E^{(2)}_{\rm m} &= \sum_{J'F'}\frac{|\langle\Upsilon\Gamma' IJ'F'M_F|N^{(1)}_0+\Delta N^{(1)}_0|\Upsilon\Gamma IJFM_F\rangle B|^2}{E_{\Upsilon\Gamma IJF} - E_{\Upsilon\Gamma' IJ'F'}} \\ &= C_{\rm m2}B^2,\end{aligned} \tag{20}$$

where $C_{\rm m2}$ is the quadratic Zeeman shift coefficient. The hyperfine level energy is $E_{IJF} = E_J + \Delta E_{\rm hfs}$, and $\Delta E_{\rm hfs}$ is given by

$$\Delta E_{\rm hfs} = \frac{1}{2}A_{\rm hfs}K + B_{\rm hfs}\frac{\frac{3}{4}K(K+1) - I(I+1)J(J+1)}{2I(2I-1)J(2J-1)}, \tag{21}$$

where $K = F(F+1) - J(J+1) - I(I+1)$, the magnetic dipole and the electric quadrupole hyperfine interaction constants $A_{\rm hfs}$ and $B_{\rm hfs}$ of the clock states in the $^{61}Ni^{12+}$ ion have been calculated in our previous work [31].

For the state with quantum number $J = 0$, the second-order Zeeman shift arises from levels separated in energy by the fine-structure splitting, while for the state with nonzero

J, it arises from nearby hyperfine levels. Accordingly, the quadratic Zeeman shift coefficient of the states with nonzero J is

$$\begin{aligned}C_{\rm m2} \approx & \frac{\langle \Upsilon\Gamma IJF' M_F|N_0^{(1)}+\Delta N_0^{(1)}|\Upsilon\Gamma IJFM_F\rangle^2}{E_{\Upsilon\Gamma IJF}-E_{\Upsilon\Gamma IJF'}} \\ & + \sum_{J'F'} \frac{\left(d^{(1)}_{\Gamma'J'}\langle \Upsilon\Gamma IJ'F'M_F|N_0^{(1)}+\Delta N_0^{(1)}|\Upsilon\Gamma IJFM_F\rangle\right)^2}{E_{\Upsilon\Gamma IJF}-E_{\Upsilon\Gamma IJF'}} \\ & + 2\sum_{J'F'} d^{(1)}_{\Gamma J'}\langle \Upsilon\Gamma IJ'F'M_F|N_0^{(1)}+\Delta N_0^{(1)}|\Upsilon\Gamma IJFM_F\rangle \\ & \times \frac{\langle \Upsilon\Gamma IJF' M_F|N_0^{(1)}+\Delta N_0^{(1)}|\Upsilon\Gamma IJFM_F\rangle}{E_{\Upsilon\Gamma IJF}-E_{\Upsilon\Gamma IJF'}} \\ & + 2\sum_{J'F'} \frac{d^{(1)}_{\Gamma'J'}\langle \Upsilon\Gamma IJ'F'M_F|N_0^{(1)}+\Delta N_0^{(1)}|\Upsilon\Gamma IJFM_F\rangle}{E_{\Upsilon\Gamma IJF}-E_{\Upsilon\Gamma IJF'}} \\ & \times \sum_{J'F'} d^{(1)}_{\Gamma'J'}\langle \Upsilon\Gamma IJ'F'M_F|N_0^{(1)}+\Delta N_0^{(1)}|\Upsilon\Gamma IJFM_F\rangle \\ = & C^{(0)}_{\rm m2}+\delta C^{(1)}_{\rm m2\,hfs}. \end{aligned} \tag{22}$$

For the state with $J=0$, it is

$$\begin{aligned}C_{\rm m2} \approx & \sum_{J'F'} \frac{\langle \Upsilon\Gamma IJ'F'M_F|N_0^{(1)}+\Delta N_0^{(1)}|\Upsilon\Gamma IJFM_F\rangle^2}{E_{\Upsilon\Gamma IJF}-E_{\Upsilon\Gamma IJ'F'}} \\ & + \sum_{J'F'} \frac{(d^{(1)}_{\Gamma'J'}\langle \Upsilon\Gamma IJ'F'M_F|N_0^{(1)}+\Delta N_0^{(1)}|\Upsilon\Gamma IJFM_F\rangle)^2}{E_{\Upsilon\Gamma IJF}-E_{\Upsilon\Gamma IJ'F'}} \\ & + 2\sum_{J'F'} d^{(1)}_{\Gamma J'}\langle \Upsilon\Gamma IJ'F'M_F|N_0^{(1)}+\Delta N_0^{(1)}|\Upsilon\Gamma IJFM_F\rangle \\ & \times \frac{\langle \Upsilon\Gamma IJ'F' M_F|N_0^{(1)}+\Delta N_0^{(1)}|\Upsilon\Gamma IJFM_F\rangle}{E_{\Upsilon\Gamma IJF}-E_{\Upsilon\Gamma IJ'F'}} \\ = & C^{(0)}_{\rm m2}+\delta C^{(1)}_{\rm m2\,hfs}. \end{aligned} \tag{23}$$

The initial term means a quadratic Zeeman shift coefficient excluding the induced effect by hyperfine interaction, while the subsequent terms represent its correction arising from the hyperfine-induced effect. The Zeeman matrix elements between hyperfine states are given by

$$\begin{aligned}&\langle \Upsilon\Gamma IJFM_F|N_0^{(1)}+\Delta N_0^{(1)}|\Upsilon\Gamma' IJ'FM_F\rangle \\ &= (-1)^{I+J'+1+F}M_F\sqrt{\frac{2F+1}{F(F+1)}}\begin{Bmatrix} J & F & I \\ F & J' & 1\end{Bmatrix} \\ &\quad\times\sqrt{2J+1}\langle \Gamma J||\boldsymbol{N}^{(1)}+\Delta\boldsymbol{N}^{(1)}||\Gamma' J'\rangle \end{aligned} \tag{24}$$

and

$$\begin{aligned}&\langle \Upsilon\Gamma IJFM_F|N_0^{(1)}+\Delta N_0^{(1)}|\Upsilon\Gamma' IJ'F-1M_F\rangle \\ &= (-1)^{I+J'+1+F}M_F\sqrt{\frac{F^2-M_F^2}{F}}\begin{Bmatrix} J & F & I \\ F-1 & J' & 1\end{Bmatrix} \\ &\quad\times\sqrt{2J+1}\langle \Gamma J||\boldsymbol{N}^{(1)}+\Delta\boldsymbol{N}^{(1)}||\Gamma' J'\rangle, \end{aligned} \tag{25}$$

where $J'=J-1,J,J+1$.

C. Electric quadrupole moments of hyperfine levels

The atomic state electric quadrupole moment is due to the atomic charge distribution deviated from spherical symmetry. The interaction between the electric quadrupole moment and the electric-field gradient generated by the electrodes of an ion trap is described by the Hamiltonian $H_{\rm Q}$,

$$H_{\rm Q}=\nabla\boldsymbol{\varepsilon}^{(2)}\cdot\boldsymbol{\Theta}^{(2)}=\sum_{q=-2}^{2}(-1)^q\nabla\varepsilon^{(2)}_q\Theta^{(2)}_{-q}. \tag{26}$$

The $q=0$ components of the tensor for the gradients of the external electric field $\nabla\boldsymbol{\varepsilon}^{(2)}$ is $\nabla\varepsilon^{(2)}_0=-\frac{1}{2}\frac{\partial\varepsilon_z}{\partial z}$. $\boldsymbol{\Theta}^{(2)}$ is the electric-quadrupole operator, and $\Theta^{(2)}_0=-\frac{e}{2}(3z^2-r^2)$ [38].

We treated the $H_{\rm Q}$ as a perturbation, since the energy shift due to $H_{\rm Q}$ is small in practice. For a given hyperfine level $|FM_F\rangle$, the energy correction is

$$\Delta E_{\rm Q}=\frac{1}{2}\frac{\partial\varepsilon_z}{\partial z}\langle FM_F|\Theta^{(2)}_0|FM_F\rangle. \tag{27}$$

Considering the wave functions of the atomic system with hyperfine mixing Eq. (9), the electric quadrupole moment of the hyperfine level $\Theta_F=\langle\Gamma F|\Theta^{(2)}_0|\Gamma F\rangle$ is

$$\begin{aligned}\Theta_F \approx & \langle \Upsilon\Gamma IJFM_F|\Theta^{(2)}_0|\Upsilon\Gamma IJFM_F\rangle \\ & + 2\sum_{\Gamma'J'} d^{(1)}_{\Gamma'J'}\langle \Upsilon\Gamma IJFM_F|\Theta^{(2)}_0|\Upsilon\Gamma' IJ'FM_F\rangle \\ = & \Theta^{(0)}_F+\delta\Theta^{(1)}_{F\,\rm hfs}, \end{aligned} \tag{28}$$

where

$$\begin{aligned}&\langle \Upsilon\Gamma IJFM_F|\Theta^{(2)}_0|\Upsilon\Gamma' IJ'FM_F\rangle \\ &= (-1)^{I+J'+1+F}\left[3M_F^2-F(F+1)\right] \\ &\quad\times\sqrt{\frac{2F+1}{(2F+3)(F+1)F(2F-1)}}\begin{Bmatrix} J & 2 & J' \\ F & I & F\end{Bmatrix} \\ &\quad\times\langle \Gamma J||\boldsymbol{\Theta}^{(2)}||\Gamma' J'\rangle. \end{aligned} \tag{29}$$

Since $\boldsymbol{\Theta}^{(2)}$ is an even-parity operator of rank 2, the electric quadrupole moments of the $3s^23p^4\ {}^3P_1\ F=1/2$ and ${}^3P_2\ F=1/2$ states in the $^{61}Ni^{12+}$ ion are strictly zero. For the electric quadrupole moments of the $3s^23p^4\ {}^3P_0\ F=3/2$ state, only contributions from the adjacent ${}^3P_2$ and ${}^1D_2$ states are included in practical calculations; others are neglected because their fractional contribution is less than 10^{-13}. In addition, the direct contribution due to the nuclear electronic quadrupole moment of ^{61}Ni ($Q=0.162\,\text{b}\approx 6.4\times10^{-9}$ a.u.) is negligible for the electric quadrupole frequency shifts of the concerned transitions in the $^{61}Ni^{12+}$ ion.

D. MCDHF method

In the MCDHF method, an electronic state wave function (ESFs) $|\Gamma JM_J\rangle$ is constructed with configuration state functions (CSFs) $|\gamma JM_J\rangle$ with the same parity, total angular momentum J, and its component along the z direction M_J [39,40]:

$$|\Gamma JM_J\rangle=\sum_{i=1}^{N_{\rm CSF}}c_i|\gamma_i JM_J\rangle, \tag{30}$$

where c_i is the mixing coefficient, and γ_i stands for other appropriate labeling of the CSF. Each CSF is a linear combination of products of one-electron Dirac orbitals. Both the mixing coefficients and the orbitals are optimized in the self-consistent field (SCF) procedure to minimize the energies of the levels concerned. Once a set of orbitals is obtained, relativistic configuration interaction (RCI) calculations can be carried out to capture more electron correlations by optimizing the mixing coefficients. In addition, the Breit interaction and leading quantum electrodynamic (QED) corrections have also been included by the RCI calculations [41].

III. COMPUTATIONAL MODEL

For the many-electron atomic system, the description of electron correlations in the computational model is crucial for the precision of the calculated atomic parameters. In the framework of the MCDHF method, the electron correlation effects are divided into first- and higher-order electron correlation effects according to the perturbation theory, and these correlations are captured by the active space approach.

In the case of Ni^{12+}, the first-order electron correlation effects were captured by the CSFs generated through the single and double (SD) excitation from the occupied orbitals in the reference configuration $3s^23p^4$ to virtual orbitals. To capture the electron correlation effect systematically, we treated the $3s$ and $3p$ orbitals as valence orbitals and others as core. Therefore, the first-order electron correlation is composed of the correlation between valence electrons (VV correlation), the correlation between core and valence electrons (CV correlation), and the correlation between the core electrons (CC correlation). In this work, the VV and CV correlation were taken into account in the SCF calculations. The SCF calculations were started from the Dirac-Hartree-Fock (DHF) approximation, where the occupied orbitals are optimized as spectroscopic orbitals. These orbitals were kept frozen in the subsequent calculations. To capture the VV and CV correlations, the configuration space was augmented by the restricted SD replacement of occupied orbitals with a set of virtual orbitals. The restriction condition is that only one core orbital can be substituted at a step. For monitoring the convergence, the virtual orbitals were enlarged and optimized layer by layer up to $n_{\max} = 12$ and $l_{\max} = 6$, where $n_{\max}$ and $l_{\max}$ are the maximum principal quantum number and the maximum angular quantum number of the virtual orbitals. Each layer consists of orbitals with different orbital angular momentum. For example, the first layer of virtual orbitals consists of $\{4s, 4p, 3d, 4f\}$ in this work. In our test calculations, it was observed that the contributions from orbitals with large orbital angular momentum l (such as $9i$, $10h$, $11g$ orbitals, etc.) were negligible for the atomic parameters concerned, hence these orbitals were not included in the set of active orbitals. The orbitals set formed in the last step of SCF calculations, labeled as CV, were fixed in RCI calculations.

The CC correlations were taken into account in RCI calculations by adding the CSFs generated through the SD excitation from the core orbitals to all virtual orbitals. To quantify the effects of various core orbitals on the physical quantities concerned, we opened up the $2p$, $2s$, and $1s$ subshells successively, and labeled corresponding calculations with CC_{2p}, CC_{2s}, and CC_{1s}, respectively. So far, all the first-order electron correlations have been captured in our calculations.

To raise the accuracy of the calculated atom parameters, the primary higher-order electron correlation was considered in our calculations. In principle, the higher-order correlation can be captured by adding the CSFs generated from the triple and quadruple (TQ) excitation. However, it is impracticable and unnecessary to include all TQ excitation CSFs in practical calculations, due to the rapid expansion of the configuration space and the minimal contributions from most of these CSFs. To control the number of CSFs and capture the dominant higher-order correlation, we employed the MR-SD approach, which further included the CSFs from the SD excitation of the multireference (MR) configuration set. Notably, the CSFs generated by the MR-SD approach are equivalent to the restricted TQ excitation from a single reference configuration. In this study the multireference (MR) configuration set, $\{3s^23p^4, 3s3p^43d, 3s^23p^23d^2, 3p^6\}$, was formed by selecting the CSFs with the weights of $|c_i| > 0.01$ in the configuration space of the CC_{1s} model. This model is marked as MR, in which the SD excitations are permitted from orbitals with $n \geqslant 2$ in the multireference configurations to the three layers of virtual orbitals. Finally, the contributions of the Breit interaction and the QED effects are evaluated based on the MR model, labeled using MR-B and MR-BQ, respectively. In practice, we employ the GRASP2018 [42] and HFSZEEMAN95 [43] packages to perform present calculations. The active orbital and the number of CSFs corresponding to computational processes are shown in Table I.

IV. RESULTS AND DISCUSSION

A. Energies

Table II shows the energies of the $3s^23p^4\ ^3P_1$, $^3P_0$, and $^1D_2$ states in the Ni^{12+} ion as functions of the computational models. It is observed that the VV and CV electron correlations contribute significantly to the fine structure of Ni^{12+} ion. Specifically, from the DF model to the CV model, the calculated energies of $^3P_1$, $^3P_0$, and $^1D_2$ states vary by 0.3%, 5%, and 8% respectively. The effects of the electron correlation between core orbitals are relatively small, as the nuclear Coulomb potential is stronger in the inner region. In this case, the total contribution of the CC correlations ($CC_{2p} + CC_{2s} + CC_{1s}$) to the energies is not more than 0.1%, 0.5%, and 0.3% for the $^3P_1$, $^3P_0$, and $^1D_2$ states, respectively. The contributions of the higher-order correlations, which involve orbitals with $n \geqslant 2$ captured in the MR model, are slightly larger than the contributions of the CC correlation. These contributions to the energies of the $^3P_1$, $^3P_0$ and $^1D_2$ states are -0.2%, -0.5%, and -0.4%, respectively. Therefore, for the calculation of the Ni^{12+} ion that required high precision, the main higher-order correlation is indispensable, while the CC correlation is necessary to reduce the uncertainties. It is well known that the effect of the Breit interaction on the fine structure of HCI is important. Our calculation demonstrates that for the Ni^{12+} ion, the effect of the Breit interaction on the energies of the $^3P_1$, $^3P_0$, and $^1D_2$ states is -2.4%, -1.3%, and 1%, respectively. The contributions of the QED effect are

TABLE I. Number of CSFs for the states with $3s^2 3p^4$ configuration of Ni^{12+} ion and the active orbital in various correlation models. AO represents the active orbital, and NCSF is the number of CSFs.

Model	AO ($n_{\max} l$)	NCSF		
		$J = 0$	$J = 1$	$J = 2$
DHF	$\{3s, 3p\}$	2	1	2
CV	$\{12s, 12p, 11d, 12f, 10g, 9h, 8i\}$	130 704	362 637	520 557
CC_{2p}	$\{12s, 12p, 11d, 12f, 10g, 9h, 8i\}$	178 648	495 326	713 217
CC_{2s}	$\{12s, 12p, 11d, 12f, 10g, 9h, 8i\}$	221 881	615 343	886 166
CC_{1s}	$\{12s, 12p, 11d, 12f, 10g, 9h, 8i\}$	279 334	774 815	1 115 484
MR	$\{5s, 5p, 5d, 5f, 5g\}$	613 794	1 709 421	2 473 599

less than a tenth of those of the Breit interaction. Additionally, the correction from the frequency-dependent Breit interaction on the energies concerned is evaluated between spectroscopic orbitals, and considered in the results from the MR-BQ model.

The level structure and transition properties of the Ni^{12+} ion were evaluated with a variety of theoretical methods [26,44–49], for the purpose of interpreting the vast amount of observational data from the solar, astrophysical, and laboratory plasma. At the bottom of Table II, we compared the calculated results with the recommended values from the National Institute of Standards and Technology (NIST) and theoretical results in the literature for the energies of states concerned in Ni^{12+} ion. Ishikawa and Vilkas [44] calculated energies of 46 states arising from the $3s^2 3p^4$, $3s3p^5$, and $3s^2 3p^3 3d$ configurations of S-like ions using multireference Møller-Plesset (MR-MP) perturbation theory. Their results have excellent agreement, within 0.2%, with the NIST values since almost all electron correlations (nondynamic and dynamic correlations), the Breit interaction, and the QED effect are captured in the calculation. By contrast, for the superstructure (SS) calculations by Bhatia and Doschek [45], only the $3s^2 3p^4$ and $3p^6$ configurations were used to optimize the atomic state wave function of even states. Therefore, the SS calculations yield differences of 8% and 4% for the $^3P_{1,0}$ and $^1D_2$ states with the NIST values. The electron correlations included in the earlier MCDHF calculations by Chou *et al.* [46], Aggarwal *et al.* [47], and Nazir *et al.* [48] are similar, only considering the main VV correlation. Therefore, the discrepancies among these results are tiny. All of their calculations differed by 1% and 4% for the $^3P_{1,0}$ and $^1D_2$ states from the NIST. In addition, Nazir *et al.* [48] also performed the flexible atomic code (FAC) calculation, and their FAC results agree well with the MCDHF calculation for the levels belonging to the configuration $3s^2 3p^4$. The higher-order correlation is neglected in the MCDHF calculations by Yu and Sahoo [26], while the CC correlation is neglected in the calculation by Wang *et al.* [49]. As shown in our calculation, the contributions of the higher-order correlation are larger than and opposite to those of the CC correlation. Thus, the results calculated by Wang *et al.* are in better agreement with the recommended values in the NIST database. It is shown that the sufficient description of electron correlations in the computational model is indispensable for calculation asked for high precision. On the whole, our calculated results are in good agreement (within 0.5%) with the recommended values in the NIST database, since sufficient electron correlations and Breit interaction are captured in our calculations. The good agreement also confirms the reliability of the computational model.

TABLE II. Energies of the $3s^2 3p^4$ $^3P_1$, $^3P_0$, and $^1D_2$ states relative to the ground state $^3P_2$ in the Ni^{12+} ion (in a.u.). Other theoretical results and the NIST values are also presented for comparison.

Model	$^3P_1$	$^3P_0$	$^1D_2$
DHF	0.0909	0.0975	0.2344
CV	0.0911	0.0930	0.2178
CC_{2p}	0.0912	0.0933	0.2181
CC_{2s}	0.0912	0.0934	0.2182
CC_{1s}	0.0912	0.0935	0.2184
MR	0.0910	0.0930	0.2174
MR-B	0.0889	0.0918	0.2153
MR-BQ	0.0890	0.0917	0.2153
	Others		
Ishikawa [44]	0.0890	0.0915	0.2140
Bhatia [45]	0.0815	0.0845	0.2220
Chou [46]	0.0884	0.0920	0.2235
Aggarwal [47]	0.0880	0.0915	0.2225
Nazir[a] [48]	0.0880	0.0915	0.2225
Nazir[b] [48]	0.0880	0.0910	0.2215
Yu [26]	0.0891	0.0923	0.2165
Wang [49]	0.0890	0.0918	0.2150
NIST [50]	0.0890	0.0914	0.2143

[a]Calculated with the MCDHF method.
[b]Calculated with FAC.

B. Hyperfine-induced Landé *g* factor and quadratic Zeeman shift

As shown in Sec. II B, only the states belonging to the $3s^2 3p^4$ configuration are considered in practical calculations, since the contributions from others are negligible. Therefore, for the $^3P_0$ $F = 3/2$ and $^3P_{1,2}$ $F = 1/2$ states the hyperfine-induced Landé g factors are

$$\delta g^{(1)}_{F\,\mathrm{hfs}}(^3P_0) = 2\frac{\langle {}^3P_0\, F M_F | N_0^{(1)} + \Delta N_0^{(1)} | {}^3P_1\, F M_F\rangle}{M_F} \times \frac{\langle {}^3P_1\, F M_F | H_{\mathrm{hfs}} | {}^3P_0\, F M_F\rangle}{E_{^3P_0} - E_{^3P_1}}, \tag{31}$$

TABLE III. Reduced off-diagonal hyperfine interaction matrix elements (in a.u.).

M1 hyperfine interaction

Model	$\langle {}^3P_1 \Vert \boldsymbol{T}^{(1)} \Vert {}^3P_0\rangle$	$\langle {}^3P_2 \Vert \boldsymbol{T}^{(1)} \Vert {}^3P_1\rangle$	$\langle {}^1D_2 \Vert \boldsymbol{T}^{(1)} \Vert {}^3P_1\rangle$	$\langle {}^1D_2 \Vert \boldsymbol{T}^{(1)} \Vert {}^3P_2\rangle$
DHF	0.31468	0.62644	0.9669	0.21191
CV	0.27027	0.58665	1.0068	0.21847
CC_{2p}	0.27303	0.58857	1.0055	0.21717
CC_{2s}	0.27403	0.58947	1.0056	0.21690
CC_{1s}	0.27603	0.59126	1.0058	0.21623
MR	0.26738	0.58255	1.0027	0.21820
MR-B	0.26829	0.58711	0.9994	0.22309
MR-BQ	0.26824	0.58678	0.9996	0.22271

E2 hyperfine interaction

Model	$\langle {}^3P_2 \Vert \boldsymbol{T}^{(2)} \Vert {}^3P_1\rangle$	$\langle {}^1D_2 \Vert \boldsymbol{T}^{(2)} \Vert {}^3P_1\rangle$	$\langle {}^1D_2 \Vert \boldsymbol{T}^{(2)} \Vert {}^3P_2\rangle$	$\langle {}^3P_2 \Vert \boldsymbol{T}^{(2)} \Vert {}^3P_0\rangle$	$\langle {}^1D_2 \Vert \boldsymbol{T}^{(2)} \Vert {}^3P_0\rangle$
DHF	46.255	10.894	29.987	33.251	−9.6898
CV	46.629	11.846	32.475	34.066	−11.733
CC_{2p}	46.570	11.820	32.404	34.009	−11.616
CC_{2s}	46.583	11.819	32.400	34.014	−11.584
CC_{1s}	46.579	11.812	32.383	34.007	−11.550
MR	46.452	11.813	32.379	33.940	−11.653
MR-B	46.401	11.583	31.786	33.786	−11.328
MR-BQ	46.396	11.598	31.822	33.792	−11.354

$$\delta g^{(1)}_{F\,\mathrm{hfs}}({}^3P_1) = 2\Bigg[\frac{\langle {}^3P_1\, FM_F|N_0^{(1)}+\Delta N_0^{(1)}|\,{}^3P_2\, FM_F\rangle}{M_F} \times \frac{\langle {}^3P_2\, FM_F|H_{\mathrm{hfs}}|\,{}^3P_1\, FM_F\rangle}{E_{{}^3P_1}-E_{{}^3P_2}} + \frac{\langle {}^3P_1\, FM_F|N_0^{(1)}+\Delta N_0^{(1)}|\,{}^1D_2\, FM_F\rangle}{M_F} \times \frac{\langle {}^1D_2\, FM_F|H_{\mathrm{hfs}}|\,{}^3P_1\, FM_F\rangle}{E_{{}^3P_1}-E_{{}^1D_2}}\Bigg], \tag{32}$$

and

$$\delta g^{(1)}_{F\,\mathrm{hfs}}({}^3P_2) = 2\Bigg[\frac{\langle {}^3P_2\, FM_F|N_0^{(1)}+\Delta N_0^{(1)}|\,{}^3P_1\, FM_F\rangle}{M_F} \times \frac{\langle {}^3P_1\, FM_F|H_{\mathrm{hfs}}|\,{}^3P_2\, FM_F\rangle}{E_{{}^3P_2}-E_{{}^3P_1}} + \frac{\langle {}^3P_2\, FM_F|N_0^{(1)}+\Delta N_0^{(1)}|\,{}^1D_2\, FM_F\rangle}{M_F} \times \frac{\langle {}^1D_2\, FM_F|H_{\mathrm{hfs}}|\,{}^3P_2\, FM_F\rangle}{E_{{}^3P_2}-E_{{}^1D_2}}\Bigg]. \tag{33}$$

The reduced off-diagonal hyperfine interaction and Zeeman matrix elements needed to calculate the $\delta g^{(1)}_{F\,\mathrm{hfs}}({}^3P_{0,1,2})$ for the $^{61}Ni^{12+}$ ion as functions of computational models are presented in Table III and Table IV, respectively. As can be seen, the first-order electron correlation related to the valence orbitals is the primary electron correlation for these matrix elements. For most of these matrix elements, the corrections attributed to the CC and higher-order correlations are relatively small and with opposite signs. The effect of Breit interaction and the QED effect on most of the matrix elements concerned is not more than 1% and 0.2%, respectively.

The hyperfine-induced g factors for the $^3P_0$ $F = 3/2$ and $^3P_{1,2}$ $F = 1/2$ states in $^{61}Ni^{12+}$ ion are presented in Table V. It is found that the tendencies of electron correlation effects

TABLE IV. Reduced Zeeman matrix elements (in a.u.).

Model	$\langle {}^3P_0 \Vert \boldsymbol{\mu}^{(1)} \Vert {}^3P_1\rangle$	$\langle {}^3P_1 \Vert \boldsymbol{\mu}^{(1)} \Vert {}^3P_2\rangle$	$\langle {}^3P_1 \Vert \boldsymbol{\mu}^{(1)} \Vert {}^1D_2\rangle$	$\langle {}^3P_2 \Vert \boldsymbol{\mu}^{(1)} \Vert {}^1D_2\rangle$	$\langle {}^3P_1 \Vert \boldsymbol{\mu}^{(1)} \Vert {}^3P_1\rangle$	$\langle {}^3P_2 \Vert \boldsymbol{\mu}^{(1)} \Vert {}^3P_2\rangle$
DHF	0.67983	0.44384	0.11035	0.14328	1.060746	1.8015
CV	0.67132	0.44179	0.11826	0.15285	1.060742	1.7961
CC_{2p}	0.67175	0.44182	0.11816	0.15273	1.060743	1.7962
CC_{2s}	0.67190	0.44183	0.11812	0.15268	1.060743	1.7963
CC_{1s}	0.67204	0.44185	0.11807	0.15262	1.060743	1.7963
MR	0.67146	0.44176	0.11837	0.15299	1.060744	1.7962
MR-B	0.67313	0.44231	0.11633	0.15053	1.060744	1.7975
MR-BQ	0.67299	0.44227	0.11648	0.15071	1.060744	1.7975

TABLE V. Hyperfine-induced Landé g factors of the $^3P_0$ $F = 3/2$ and $^3P_{1,2}$ $F = 1/2$ states in $^{61}Ni^{12+}$ ion. Numbers in square brackets stand for the power of 10 and in parentheses for the uncertainties.

	$\delta g^{(1)}_{F\,\mathrm{hfs}}(^3P_0\ F = 3/2)$		$\delta g^{(1)}_{F\,\mathrm{hfs}}(^3P_1\ F = 1/2)$		$\delta g^{(1)}_{F\,\mathrm{hfs}}(^3P_2\ F = 1/2)$	
Model	Cal.	Rev.	Cal.	Rev.	Cal.	Rev.
DHF	7.451 [−5]	2.080 [−4]	9.189 [−6]	9.129 [−6]	−1.232 [−5]	−1.266 [−5]
CV	2.210 [−4]	1.764 [−4]	8.097 [−6]	8.320 [−6]	−1.199 [−5]	−1.227 [−5]
CC_{2p}	2.012 [−4]	1.783 [−4]	8.126 [−6]	8.347 [−6]	−1.200 [−5]	−1.228 [−5]
CC_{2s}	1.950 [−4]	1.790 [−4]	8.138 [−6]	8.360 [−6]	−1.201 [−5]	−1.229 [−5]
CC_{1s}	1.903 [−4]	1.804 [−4]	8.161 [−6]	8.384 [−6]	−1.202 [−5]	−1.231 [−5]
MR	2.105 [−4]	1.746 [−4]	8.048 [−6]	8.262 [−6]	−1.194 [−5]	−1.220 [−5]
MR-B	1.429 [−4]	1.756 [−4]	8.422 [−6]	8.386 [−6]	−1.227 [−5]	−1.226 [−5]
MR-BQ	1.5(2) [−4]	1.76(6) [−4]	8.4 (1) [−6]	8.4 (1) [−6]	−1.22 (1) [−5]	−1.22 (1) [−5]

on the g factors are similar to those on the matrix elements and energies. In this work, the sufficient electron correlations, Breit interaction, and the QED effect were taken into account systematically. Thus, the higher-order electron correlation that was neglected in the computational models is the dominant source of uncertainty for our calculated result. The upper limit on the effects of this correlation should be smaller than the higher-order correlation included in the calculation, since the stronger nuclear Coulomb potential is in the inner region. Conservatively, we treated the contribution of the higher-order correlations captured in the MR model as the uncertainty due to the neglected higher-order correlations. The "truncation" uncertainties due to the finite number of virtual orbitals were evaluated according to the convergence trends of the various correlations. The final uncertainty shown in parentheses in Table V is the square root of the sum of the squares of the individual uncertainties. It can be seen that the uncertainty of $\delta g^{(1)}_{F\,\mathrm{hfs}}(^3P_0\ F = 3/2)$ reaches 15%. This large uncertainty mainly results from the energy interval between $^3P_1$ and $^3P_0$ states $\Delta E_{^3P_0 - {}^3P_1}$.

It was found that the $\Delta E_{^3P_0 - {}^3P_1}$ is much more sensitive to the electron correlation, Breit interaction, and the QED effect than the other energies used in this work. In fact, our calculated $\Delta E_{^3P_0 - {}^3P_1}$ deviates from the NIST value by 16%. To improve the $\Delta E_{^3P_0 - {}^3P_1}$, one can optimize $J = 0$ and $J = 1$ terms separately. Nevertheless, the resulting orbital in this way are nonorthogonal with each other, and the off-diagonal Zeeman and hyperfine interaction matrix elements cannot be dealt with using the standard Racah technique. We revised the calculated results using the energy values from the NIST database, and marked as "Rev." in Table V. The uncertainty of the revised $\delta g^{(1)}_{F\,\mathrm{hfs}}(^3P_0\ F = 3/2)$ is decreased to not more than 4%. Moreover, the calculated result (labeled as "Cal.") is in agreement with the revised result. For the $\delta g^{(1)}_{F\,\mathrm{hfs}}(^3P_1\ F = 1/2)$ and $\delta g^{(1)}_{F\,\mathrm{hfs}}(^3P_2\ F = 1/2)$, the calculated results are found to be in excellent agreement with the revised results, and with uncertainties less than 2%.

For the clock transitions of the $^{61}Ni^{12+}$ ion, the first-order Zeeman shift can be canceled by measuring two transitions with the opposite magnetic quantum number M_F and averaging the frequencies. In order to evaluate the second-order Zeeman shift, we evaluated the quadratic Zeeman shift coefficient C_{m2} of the magnetic substates with $|M_F| = 1/2$ for the $^3P_0$ $F = 3/2$ and $^3P_{1,2}$ $F = 1/2$ states and show this in Table VI. It is found that the calculated C_{m2} are smaller than the estimated values, which are independent of M_F by $C_{\mathrm{m2}} \sim (g_J\mu_B - g_I\mu_N)^2/h^2A_{\mathrm{hfs}}$. The discrepancy is mainly due to the fact that only the magnetic dipole hyperfine interaction is considered for the estimated result. As we show in Table VI, we revised the estimated results by $C_{\mathrm{m2}} \sim (g_J\mu_B - g_I\mu_N)^2/\Delta E_F$, where ΔE_F represents the hyperfine splitting, and the revised estimate values agree well with our calculated values. The hyperfine-induced quadratic Zeeman shift coefficients $\delta C^{(1)}_{\mathrm{m2\,hfs}}$ for magnetic substates of $^3P_0$ $F = 3/2$ and $^3P_{1,2}$ $F = 1/2$ states are evaluated. It is shown that the hyperfine-induced effect influences the C_{m2} at the level of 10^{-4} for the $^3P_0$ $F = 3/2$ and $^3P_1$ $F = 1/2$ states, and the level of 10^{-7} for the $^3P_2$ $F = 1/2$ state.

As shown in Fig. 2, we evaluated the relative quadratic Zeeman shifts of clock transitions and the correction caused by the hyperfine-induced effect as a function of the magnetic field B. It is observed that under a magnetic field of $B = 1\,\mu\mathrm{T}$, the relative quadratic Zeeman shifts are 2.0×10^{-16} and 1.2×10^{-16} for the M1 transition $^3P_1 - {}^3P_2$ and E2 transition $^3P_0 - {}^3P_2$ in Ni^{12+} ion, respectively. Additionally, the relative quadratic Zeeman shifts induced by the hyperfine interaction are at the level of 10^{-20} and 10^{-23} for the M1 and E2 transitions, respectively. Therefore, to achieve a Ni^{12+} clock with the fractional uncertainties below 10^{-19} level, it is crucial

TABLE VI. Quadratic Zeeman shift coefficient C_{m2} (in $\mathrm{Hz/T^2}$) and hyperfine-induced correction $\delta C^{(1)}_{\mathrm{m2\,hfs}}$ of the $^3P_0$ $F = 3/2$ and $^3P_{1,2}$ $F = 1/2$ states in $^{61}Ni^{12+}$ ion. Numbers in square brackets stand for the power of 10.

	$^3P_0$ $F = 3/2$	$^3P_1$ $F = 1/2$	$^3P_2$ $F = 1/2$
C_{m2}[a]		≈ 3.5 [12]	≈ 1.4 [11]
C_{m2}[b]		∼ 2.1 [11]	∼ 7.5 [10]
	$^3P_0$ $F = 3/2$ $\lvert M_F\rvert = 1/2$	$^3P_1$ $F = 1/2$ $\lvert M_F\rvert = 1/2$	$^3P_2$ $F = 1/2$ $\lvert M_F\rvert = 1/2$
C_{m2}[c]	5.1 [6]	1.2 [11]	7.5 [10]
$\delta C^{(1)}_{\mathrm{m2\,hfs}}$	2.8 [3]	2.1 [7]	4.1 [4]

[a]Estimated with $C_{\mathrm{m2}} \sim (g_J\mu_B - g_I\mu_N)^2/h^2A_{\mathrm{hfs}}$.
[b]Revised value with $C_{\mathrm{m2}} \sim (g_J\mu_B - g_I\mu_N)^2/\Delta E_F$.
[c]Calculated with Eqs. (22) and (23).

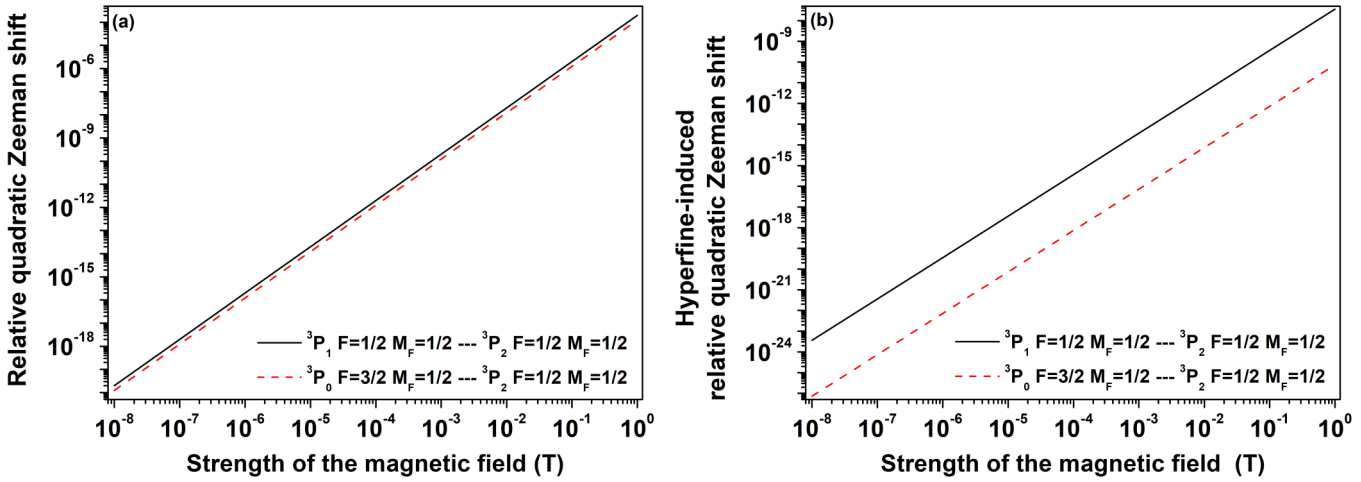

FIG. 2. Relative quadratic Zeeman shifts (a) and the correction of the hyperfine-induced effect on the relative quadratic Zeeman shifts (b) of clock transitions in $^{61}Ni^{12+}$ ion (in logarithmic scale).

to identify precisely the hyperfine-induced quadratic Zeeman shift when the magnetic field exceeds 1 μT.

C. Hyperfine-induced electric quadrupole moments

As mentioned previously, the electric quadrupole moments of the states with $F < 1$, $^3P_1$ $F = 1/2$ and $^3P_2$ $F = 1/2$, are zero. For the hyperfine induced electric quadrupole moments of the $^3P_0$ $F = 3/2$ state, only the $3s^2 3p^4$ $^3P_2$ and $^1D_2$ states are considered in practical calculations:

$$\delta\Theta^{(1)}_{F_{\rm hfs}}(^3P_0) = 2\left[\frac{\langle {}^3P_0\, FM_F|\Theta^{(2)}_0|\,{}^3P_2\, FM_F\rangle\langle {}^3P_2\, FM_F|H_{\rm hfs}|\,{}^3P_0\, FM_F\rangle}{E_{^3P_0}-E_{^3P_2}} + \frac{\langle {}^3P_0\, FM_F|\Theta^{(2)}_0|\,{}^1D_2\, FM_F\rangle\langle {}^1D_2\, FM_F|H_{\rm hfs}|\,{}^3P_0\, FM_F\rangle}{E_{^3P_0}-E_{^1D_2}}\right]. \tag{34}$$

We present the $\delta\Theta^{(1)}_{F_{\rm hfs}}(^3P_0\ F = 3/2)$ and the reduced off-diagonal electric quadrupole matrix elements needed as functions of the computational models in Table VII. It can be seen the electron correlation related to the valence orbitals and the Breit interaction are crucial to the $\delta\Theta^{(1)}_{F_{\rm hfs}}(^3P_0\ F = 3/2)$. The contribution of the CC correlations and the QED effect are relatively small but necessary to reduce the uncertainties. The uncertainty of the $\delta\Theta^{(1)}_{F_{\rm hfs}}(^3P_0\ F = 3/2)$ is also composed of "truncation" uncertainties and the uncertainty due to the neglected higher-order correlations. Moreover, the uncertainty due to the neglected higher-order correlations is the contribution of the higher-order correlations captured in the MR model. Our calculated $\delta\Theta^{(1)}_{F_{\rm hfs}}(^3P_0\ F = 3/2)$ with uncertainty of less than 0.3% is in excellent agreement with the revised value using the energy values from the NIST database, since sufficient electron correlations, the Breit interaction, and the QED effect are captured in our calculations.

The electric quadrupole shift caused by the interaction between the electric quadrupole moments of the clock states with the gradient of the electric field is one of the main systematic shifts in the atomic clock. As shown in Fig. 3, we evaluated the relative electric quadrupole shifts of clock transitions as a function of the gradient of the environmental electric field. It can be seen that compared with the transitions between fine levels, the electric quadrupole shifts of transition between hyperfine levels are significantly suppressed. Specifically, the electric quadrupole shifts of the M1 transition $^3P_1$ $F = 1/2 - {}^3P_2$ $F = 1/2$ are removed strictly.

TABLE VII. Hyperfine-induced electric quadrupole moments of the $^3P_0$ $F = 3/2$ state $\delta\Theta^{(1)}_{F_{\rm hfs}}(^3P_0\ F = 3/2)$ (in a.u.) and the electric quadrupole matrix elements (in a.u.). Numbers in square brackets stand for the power of 10 and in parentheses for the uncertainties.

			$\delta\Theta^{(1)}_{F_{\rm hfs}}(^3P_0\ F = 3/2)$	
Model	$\langle {}^3P_0 \|\boldsymbol{\Theta}^{(2)}\| {}^3P_2\rangle$	$\langle {}^3P_0 \|\boldsymbol{\Theta}^{(2)}\| {}^1D_2\rangle$	Cal.	Rev.
DHF	−0.33152	0.043673	−2.845 [−7]	−3.031 [−7]
CV	−0.31531	0.048476	−2.869 [−7]	−2.921 [−7]
CC_{2p}	−0.31629	0.048296	−2.868 [−7]	−2.927 [−7]
CC_{2s}	−0.31660	0.048227	−2.869 [−7]	−2.931 [−7]
CC_{1s}	−0.31689	0.048165	−2.868 [−7]	−2.933 [−7]
MR	−0.31573	0.048327	−2.864 [−7]	−2.915 [−7]
MR-B	−0.31506	0.047152	−2.887 [−7]	−2.901 [−7]
MR-BQ	−0.31512	0.047255	−2.889 (7) [−7]	−2.90 (2) [−7]

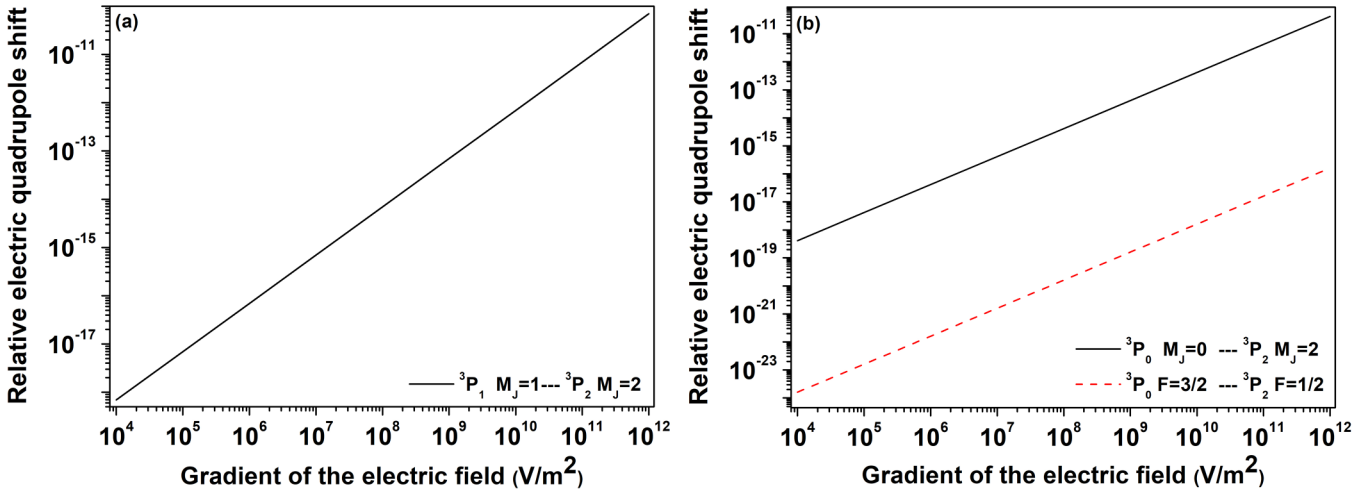

FIG. 3. Relative electric quadrupole shift of the M1 transition $^3P_1$ $M_J = 1 - {}^3P_2$ $M_J = 2$ (a) and the E2 transitions (b) $^3P_0$ $M_J = 0 - {}^3P_2$ $M_J = 2$ and $^3P_0$ $F = 3/2 - {}^3P_2$ $F = 1/2$ in the $^{61}Ni^{12+}$ ion (in logarithmic scale). The relative electric quadrupole shift of the transition $^3P_1$ $F = 1/2 - {}^3P_2$ $F = 1/2$ is zero.

Assuming the gradient of the environmental electric field is 10^8 V/m^2, the relative electric quadrupole shifts of the E2 transition can be reduced from 4.2×10^{-15}(for $^3P_0$ $M_J = 0 - {}^3P_2$ $M_J = 2$) to 1.6×10^{-20} (for $^3P_0$ $F = 3/2 - {}^3P_2$ $F = 1/2$). It means that for achieving the optical clock with the fractional uncertainties below 10^{-19}, the hyperfine-induced electric quadrupole shift is non-negligible once the gradient of the environmental electric field exceeds 10^8 V/m^2.

V. CONCLUSION

In summary, the hyperfine-induced effect on the two candidate clock transitions in the $^{61}Ni^{12+}$ ion was investigated in the weak field approximation. We carried out *ab initio* calculations on the hyperfine-induced corrections to Landé g factors of $^3P_0$ $F = 3/2$ and $^3P_{1,2}$ $F = 1/2$ states, and to the electronic quadrupole moment of the $^3P_0$ $F = 3/2$ state using the MCDHF method. Based on the investigation of the sensitivity of the atomic parameters concerned to electron correlations, the Breit interaction, and the QED effect, the computational uncertainties were estimated. Combined with the environmental conditions, the relative quadratic Zeeman shifts and electric quadrupole shifts were evaluated. For the $^3P_1 - {}^3P_2$ and $^3P_0 - {}^3P_2$ transitions in the $^{61}Ni^{12+}$ ion, the hyperfine interaction introduces corrections to the relative quadratic Zeeman shift by factors of 2×10^{-4} and 6×10^{-7}, respectively. Additionally, the hyperfine interaction strictly eliminates the electric quadrupole shift of the M1 transition, and significantly reduces the electric quadrupole frequency shift for the E2 transition by a factor of 4×10^{-6}. Therefore, for an $^{61}Ni^{12+}$ optical clock with a precision better than 10^{-19}, it is crucial to determine the hyperfine-induced effects accurately, when the magnetic field exceeds 1 μT or the gradient of the environmental electric field exceeds 10^8 V/m^2.

ACKNOWLEDGMENTS

This work was supported by the National Natural Science Foundation of China (Grants No. 12204211, No. 11934014, and No. 12274423) and Institute of Applied Physics and Computational Mathematics (Contract No. HXO2023-55). The authors thank Ji-guang Li, Hua Guan, Li-yan Tang, and Ke-lin Gao for many useful discussions. Numerical calculation were carried out on the APM-Theoretical Computing Cluster(APM-TCC) and the Computing Center in Xi'an.

[1] A. D. Ludlow, M. M. Boyd, J. Ye, E. Peik, and P. O. Schmidt, Rev. Mod. Phys. **87**, 637 (2015).
[2] T. Rosenband, D. B. Hume, P. O. Schmidt, C. W. Chou, A. Brusch, L. Lorini, W. H. Oskay, R. E. Drullinger, T. M. Fortier, J. E. Stalnaker *et al.*, Science **319**, 1808 (2008).
[3] R. M. Godun, P. B. R. Nisbet-Jones, J. M. Jones, S. A. King, L. A. M. Johnson, H. S. Margolis, K. Szymaniec, S. N. Lea, K. Bongs, and P. Gill, Phys. Rev. Lett. **113**, 210801 (2014).
[4] M. S. Safronova, D. Budker, D. DeMille, D. F. J. Kimball, A. Derevianko, and C. W. Clark, Rev. Mod. Phys. **90**, 025008 (2018).
[5] W. F. McGrew, X. Zhang, R. J. Fasano, S. A. Schäffer, K. Beloy, D. Nicolodi, R. C. Brown, N. Hinkley, G. Milani, M. Schioppo *et al.*, Nature (London) **564**, 87 (2018).
[6] T. Bothwell, D. Kedar, E. Oelker, J. M. Robinson, S. L. Bromley, W. L. Tew, J. Ye, and C. J. Kennedy, Metrologia **56**, 065004 (2019).
[7] N. Huntemann, C. Sanner, B. Lipphardt, C. Tamm, and E. Peik, Phys. Rev. Lett. **116**, 063001 (2016).
[8] Y. Huang, B. Zhang, M. Zeng, Y. Hao, Z. Ma, H. Zhang, H. Guan, Z. Chen, M. Wang, and K. Gao, Phys. Rev. Appl. **17**, 034041 (2022).
[9] S. M. Brewer, J. S. Chen, A. M. Hankin, E. R. Clements, C. W. Chou, D. J. Wineland, D. B. Hume, and D. R. Leibrandt, Phys. Rev. Lett. **123**, 033201 (2019).

[10] A. Derevianko, V. A. Dzuba, and V. V. Flambaum, Phys. Rev. Lett. **109**, 180801 (2012).

[11] V. I. Yudin, A. V. Taichenachev, and A. Derevianko, Phys. Rev. Lett. **113**, 233003 (2014).

[12] M. G. Kozlov, M. S. Safronova, J. R. Crespo López-Urrutia, P. O. Schmidt, and P. O. Schmidt, Rev. Mod. Phys. **90**, 045005 (2018).

[13] K. Beloy, V. A. Dzuba, and S. M. Brewer, Phys. Rev. Lett. **125**, 173002 (2020).

[14] K. Beloy, Phys. Rev. Lett. **127**, 013201 (2021).

[15] S. G. Porsev, U. I. Safronova, M. S. Safronova, P. O. Schmidt, A. I. Bondarev, M. G. Kozlov, I. I. Tupitsyn, and C. Cheung, Phys. Rev. A **102**, 012802 (2020).

[16] J. C. Berengut, V. A. Dzuba, and V. V. Flambaum, Phys. Rev. Lett. **105**, 120801 (2010).

[17] N.-H. Rehbehn, M. K. Rosner, H. Bekker, J. C. Berengut, P. O. Schmidt, S. A. King, P. Micke, M. F. Gu, R. Müller, A. Surzhykov, and J. R. C. López-Urrutia, Phys. Rev. A **103**, L040801 (2021).

[18] S. O. Allehabi, V. A. Dzuba, and V. V. Flambaum, Phys. Rev. A **106**, 032807 (2022).

[19] Y. M. Yu, B. K. Sahoo, and B. B. Suo, Front. Phys. **11**, 1104848 (2023).

[20] N. H. Rehbehn, M. K. Rosner, J. C. Berengut, P. O. Schmidt, T. Pfeifer, M. F. Gu, and J. R. C. López-Urrutia, Phys. Rev. Lett. **131**, 161803 (2023).

[21] V. A. Dzuba and V. V. Flambaum, Phys. Rev. A **109**, L021101 (2024).

[22] P. Micke, T. Leopold, S. A. King, E. Benkler, L. J. Spieß, L. Schmöger, M. Schwarz, J. R. Crespo López-Urrutia, and P. O. Schmidt, Nature (London) **578**, 60 (2020).

[23] L. Schmöger, O. O. Versolato, M. Schwarz, M. Kohnen, A. Windberger, B. Piest, S. Feuchtenbeiner, J. Pedregosa-Gutierrez, T. Leopold, P. Micke *et al.*, Science **347**, 1233 (2015).

[24] S. A. King, L. J. Spieß, P. Micke, A. Wilzewski, T. Leopold, E. Benkler, R. Lange, N. Huntemann, A. Surzhykov, V. A. Yerokhin *et al.*, Nature (London) **611**, 43 (2022).

[25] H. Bekker, A. Borschevsky, Z. Harman, C. H. Keitel, T. Pfeifer, P. O. Schmidt, J. R. Crespo López-Urrutia, and J. C. Berengut, Nat. Commun. **10**, 5651 (2019).

[26] Y. M. Yu and B. K. Sahoo, Phys. Rev. A **97**, 041403(R) (2018).

[27] S. Y. Liang, T. X. Zhang, H. Guan, Q. F. Lu, J. Xiao, S. L. Chen, Y. Huang, Y. H. Zhang, C. B. Li, Y. M. Zou *et al.*, Phys. Rev. A **103**, 022804 (2021).

[28] Y. M. Yu, D. Pan, S. L. Chen, B. Arora, H. Guan, K. L. Gao, and J. B. Chen, Atoms **10**, 123 (2022).

[29] S. L. Chen, Z. Q. Zhou, J. G. Li, T. X. Zhang, C. B. Li, T. Y. Shi, Y. Huang, K. L. Gao, and H. Guan, Phys. Rev. Res. **6**, 013030 (2024).

[30] K. Kromer, C. Lyu, M. Door, P. Filianin, Z. Harman, J. Herkenhoff, P. Indelicato, C. H. Keitel, D. Lange, Y. N. Novikov *et al.*, Phys. Rev. Lett. **131**, 223002 (2023).

[31] T. X. Zhang, Y. H. Zhang, C. B. Li, and T. Y. Shi, Chin. Phys. B **30**, 013101 (2021).

[32] T. X. Zhang, B. Q. Lu, J. G. Li, C. B. Li, H. Chang, T. Y. S. Shi, and Z. H. Lu, J. Quant. Spectrosc. Radiat. Transfer **266**, 107562 (2021).

[33] I. Lindgren, Rep. Prog. Phys. **47**, 345 (1984).

[34] P. Jönsson, F. A. Parpia, and C. F. Fischer, Comput. Phys. Commun. **96**, 301 (1996).

[35] N. J. Stone, At. Data Nucl. Data Tables **90**, 75 (2005).

[36] K. T. Cheng and W. J. Childs, Phys. Rev. A **31**, 2775 (1985).

[37] M. Andersson and P. Jönsson, Comput. Phys. Commun. **178**, 156 (2008).

[38] W. M. Itano, J. Res. Natl. Inst. Stand. Technol. **105**, 829 (2000).

[39] I. P. Grant, *Relativistic Quantum Theory of Atoms and Molecules: Theory and Computation* (Springer Science & Business Media, New York, 2007).

[40] C. F. Fischer, M. Godefroid, T. Brage, P. Jönsson, and G. Gaigalas, J. Phys. B **49**, 182004 (2016).

[41] J. Li, P. Jönsson, M. Godefroid, C. Dong, and G. Gaigalas, Phys. Rev. A **86**, 052523 (2012).

[42] C. Froese Fischer, G. Gaigalas, P. Jönsson, and J. Bieroń, Comput. Phys. Commun. **237**, 184 (2019).

[43] W. Li, J. Grumer, T. Brage, and P. Jönsson, Comput. Phys. Commun. **253**, 107211 (2020).

[44] Y. Ishikawa and M. J. Vilkas, Phys. Rev. A **78**, 042501 (2008).

[45] A. Bhatia and G. Doschek, At. Data Nucl. Data Tables **68**, 49 (1998).

[46] H. Chou, J. Chang, Y. Chang, and K. Huang, At. Data Nucl. Data Tables **62**, 77 (1996).

[47] K. Aggarwal, F. Keenan, and A. Msezane, At. Data Nucl. Data Tables **85**, 453 (2003).

[48] R. T. Nazir, M. A. Bari, M. Bilal, S. Sardar, M. H. Nasim, and M. Salahuddin, Chin. Phys. B **26**, 023102 (2017).

[49] K. Wang, C. X. Song, P. Jönsson, G. D. Zanna, S. Schiffmann, M. Godefroid, G. Gaigalas, X. H. Zhao, R. Si, C. Y. Chen, and J. Yan, Astrophys. J. Suppl. Ser. **239**, 30 (2018).

[50] A. Kramida, Y. Ralchenko, J. Reader, and NIST ASD Team, NIST Atomic Spectra Database (ver. 5.7.1), https://physics.nist.gov/asd. (2019).